ACS Catalysis

Research Article

pubs.acs.org/acscatalysis

Highly Dispersed Pd on Co−B Amorphous Alloy: Facile Synthesis via Galvanic Replacement Reaction and Synergetic Effect between Pd and Co

Jinqiang Ma,[†] Liang Xu,[†] Lei Xu,[†] Hao Wang,[†] Sen Xu,[†] Hexing Li,[†] Songhai Xie,[‡] and Hui Li*[,†]

[†]The Education Ministry Key Lab of Resource Chemistry and Shanghai Key Laboratory of Rare Earth Functional Materials, Shanghai Normal University, Shanghai 200234, P. R. China

[‡]Department of Chemistry, Fudan University, Shanghai 200433, P. R. China

ABSTRACT: In this paper, uniform Co−B amorphous alloy nanospheres with an average particle size of 50 nm were synthesized by chemical reduction of cobalt ion with borohydride in aqueous solution containing Bu_4PBr and KCl. Then, Pd was introduced into this system by galvanic replacement reaction (GRR) between Co and Na_2PdCl_4. Pd/Co−B catalysts with different Pd content could be obtained via adjusting the amount of Na_2PdCl_4 in reaction mixture. The crystal structure, morphology, and surface electronic state of as-prepared catalysts were characterized by XRD, TEM, XPS, and H_2-TPD. During the liquid-phase hydrogenation of 2-ethyl-2-hexenaldehyde, the as-prepared Pd/Co−B catalysts exhibited extremely active and more selectivity to 2-ethyl-1-hexanol than the monometallic Pd and Co−B amorphous alloy, showing potential application in industry. The enhanced performances could be attributed to the highly dispersed Pd on the surface of Co−B prepared by GRR and the synergetic effect between Pd and Co.

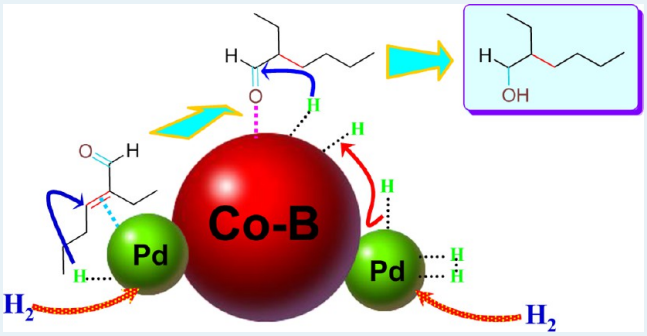

KEYWORDS: *Pd/Co−B, bimetallic catalyst, galvanic replacement reaction, hydrogenation, 2-ethyl-2-hexenaldehyde, 2-ethyl-1-hexanol*

INTRODUCTION

2-Ethyl-1-hexanol (EHO) is a valuable synthetic alcohol used as a synthon for the manufacture of ester plasticizers, coating materials, adhesives, printing inks, and impregnating agents or as an additive in foods and beverages as a volatile flavor.[1] Nowadays, practically all of the EHO is produced via the hydrogenation of 2-ethyl-2-hexenaldehyde (EHEA) with a base metal catalyst (Scheme 1).[2,3] Catalytic hydrogenation of EHEA can be performed in both the gas- and the liquid-phase. The former includes harsh reaction conditions (373−523 K and hydrogen pressures up to 3.5 MPa);[1] meanwhile, one critical issue associated with such process is the partial hydrogenation which results in a mixture of EHO and 2-ethyl-hexanal (EHA) as well as 2-ethyl-2-hexenol (EHEO).[4] The unsaturated alcohol, EHEO, is particularly undesirable because it is difficult to separate EHO by distillation. To produce pure EHO, industrially, processes for the two-step hydrogenation of EHEA were frequently performed. Generally, in the first step reaction, copper chromite catalysts are mainly employed to catalyze the hydrogenation of EHEA in the vapor phase. In the second step reaction, the condensed mixtures are then reacted further with hydrogen in the presence of another catalytic system, such as modified copper, nickel-, or palladium-based catalysts.[5−7] Obviously, the present industrial processes for the production of EHO display some drawbacks in their complicated operations (two-step process), high energy consumption (harsh reaction conditions), and environmentally unfriendliness (usage of Cr). Therefore, the development of efficient and environmentally benign catalyst that permits the synthesis of pure EHO via one-step hydrogenation of EHEA in liquid-phase seems a promising option to tackle these problems.

Amorphous alloys represent a new class of environmentally friendly catalysts with higher activity, better selectivity and stronger sulfur resistance than their crystalline counterparts owing to their unique short-range ordered but long-range

Scheme 1. Possible Reaction Pathways for EHEA Hydrogenation

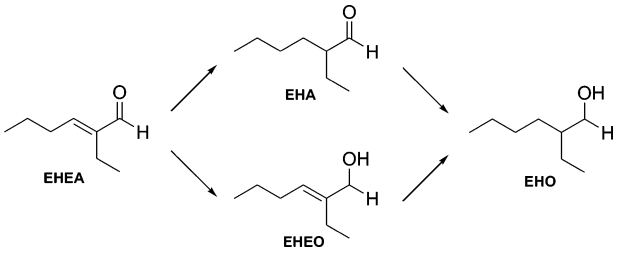

Received: January 27, 2013
Revised: April 3, 2013
Published: April 9, 2013

disordered structure.[8] As heterogeneous catalysts, amorphous alloys have been widely studied because of their excellent catalytic performances.[8−13] Our previous studies have proved Co−B amorphous alloys to be excellent catalysts for the hydrogenation of aldehyde.[14−18] However, the preliminary study revealed that the EHO obtained by the liquid-phase hydrogenation of EHEA over Co−B amorphous alloy still contained detectable amount of EHEO. Therefore, a key issue for this study is to introduce other active sites, which can not only enhance the catalytic activity of the catalytic system for EHEA hydrogenation, but also allow for the elimination of the unsaturated alcohol intermediate. Apparently, palladium is the most promising candidate because it is known as one of the best catalysts for the hydrogenation of C=C bonds.[19] Co-reduction of mixed metal salts is the most common method for synthesis of bimetallic compounds; however, it is difficult to simultaneously control the reduction and nucleation process of two kinds of metals because of the difference in their redox potential and chemical behaviors.[20] The higher standard reduction potential of the $PdCl_4^{2-}$/Pd pair (0.59 V vs standard hydrogen electrode, SHE) than that of the Co^{2+}/Co pair (−0.28 V vs SHE) will be anticipated to lead to Pd-rich core/Co-rich shell particles.[20] Considering that hydrogenation reactions occur on the surface of catalysts, a large fraction of Pd in the core of the nanoparticle is wasted and undesirable.[21] Moreover, co-reduction of the mixture of Pd^{2+} and Co^{2+} with borohydride in the present of a large amount of surfactant would result in partial oxidation of Co species.[22] In this case, design and synthesis of nanoparticles with high surface exposure of Pd represents a promising way to economize expensive Pd metal in the preparation of bimetallic Pd−Co catalyst.

The approach based on galvanic replacement reaction (GRR) provides a very facile and effective method for generating bimetallic nanoparticle with noble metal-rich surface.[23] By using GRR, Wang et al. prepared several Pd-based bimetallic Pd/M (M = Co, Ni, or Cu) catalysts, which delivered enhanced catalytic activity in cyclohexen self-hydrogenation due to the monolayer-dispersion of Pd on the non-noble metal surface.[24] Soon afterward, Wu et al. reported the synthesis of Pd/Ni−B bimetallic nanoparticle catalyst by GRR, which showed better catalytic activity and stability in the hydrodechlorination of chlorobenzene compared to those over the reference catalysts.[25] Despite effectiveness, the non-noble metals in the above-mentioned Pd/M systems were only used as inert "support" which were inactive for the performed catalytic reactions.[24,25] Consequently, the possible synergetic properties between two transition metals was still not clearly illustrated. In the present work, highly dispersed Pd on Co−B amorphous alloy was prepared by GRR. During the liquid-phase hydrogenation of EHEA, the as-prepared Pd/Co−B catalysts exhibited extremely higher activity and selectivity than the monometallic Co−B and Pd catalysts. More importantly, results from catalytic evaluation revealed "bi-site effect" in which both metals in Pd/Co−B play specific role with respect to the reactants. The correlation of the catalytic performances to the structural properties has been tentatively established.

EXPERIMENTAL PROCEDURES

Catalyst Preparation. All of the chemicals used in this experiment were analytical grade and used without further purification. Co−B amorphous alloy was prepared by a modified chemical reduction method, as we reported recently.[18] First, an aqueous solution of $CoCl_2$ (34 mL, 0.10 M) is added into an aqueous solution of Bu_4PBr (340 mL, 0.050 M). Then, 140 g of KCl is added to the above solution to form a saturated solution. In our recent work,[18] we had demonstrated that both Bu_4PBr and KCl play a key role in fabricating monodisperse and uniformly spherical Co−B nanoparticles. Thereafter, an aqueous solution of KBH_4 (27 mL, 0.50 M) is added dropwise under vigorous stirring at 273 K. After reaction is complete, the black precipitate is washed free from Cl^-, Br^- or K^+ ions with deionized water until a pH ∼ 7 is achieved. Pd deposited on Co−B amorphous alloy is prepared according to the following galvanic replacement method. The purified Co−B nanoparticles are redispersed in deionized water and sonicated for 30 min. Then, a desired amount of Na_2PdCl_4 (1.0 mM) aqueous solution is added into the above suspension through a syringe pump at a rate of 0.4 mL/min under vigorous stirring. After 30 min, the resulting solid is washed with deionized water three times followed by three washing with ethanol (EtOH), and finally soaked in EtOH until use. The as-prepared Pd−Co samples are denoted as *x* wt %-Pd/Co−B-GR, with *x* wt % referring to the Pd content and the suffix "-GR" means galvanic replacement method. For comparison, the reference Pd−Co−B and Pd catalysts are also synthesized. The reference Pd−Co−B catalyst is prepared by co-reduction of an aqueous solution containing $CoCl_2$ and Na_2PdCl_4. The as-prepared catalyst is denoted as *y* wt %−Pd−Co−B-CR, where *y* wt % refers to the Pd content and the suffix "-CR" means co-reduction method. Pd catalyst is prepared through chemical reduction of Na_2PdCl_4 aqueous solution with KBH_4 aqueous solution.

Catalyst Characterization. The bulk composition and Pd loading were analyzed by means of inductively coupled plasma (ICP; Varian VISTA-MPX). The remaining contents of ions were detected by energy-dispersive X-ray spectroscopy (EDS, Bruker QUANTAX 400) on a field emission scanning electron micrograph (FESEM; HITACHI S4800). The amorphous structure was determined by both X-ray diffraction (XRD; Rigaku D/Max-RB with Cu Kα radiation) and selective area electronic diffraction (SAED; JEOL JEM-2100). Transmission electron microscopy (TEM) and high-resolution TEM (HRTEM) images were obtained on a JEOL JEM-2100 electron microscope, operated at an acceleration voltage of 200 kV. X-ray photoelectron spectroscopy (XPS) measurements were performed on a ULVAC-PHI PHI5000 VersaProbe system using Al Kα radiation, during which all samples were dried and pretreated *in situ* in pure Ar atmosphere to avoid oxidation. All the binding energy (BE) values were calibrated by using C 1s = 284.6 eV) as a reference. Hydrogen temperature-programmed desorption (H_2-TPD) curves were obtained on a Micromeritics AutoChem II 2920 instrument which can be described as follows. The catalyst surface was purged under an argon flow (purity of 99.997%, treated with an Alltech Oxy-Trap column) at 523 K for 2 h. The pretreated sample was cooled down to room temperature under argon atmosphere, and hydrogen was preadsorbed by the sample at room temperature for 24 h to ensure maximum uptake. The hydrogen steam was then replaced with a carrier gas of argon, which was kept for 2 h in order to purge the gaseous and physisorbed hydrogen away from the catalyst cell. Then, hydrogen desorption was carried out by raising the temperature at a ramping rate of 10 K/min in which the released H_2 was determined by TCD.

Activity Test. Liquid-phase hydrogenation of EHEA was carried out in a 250 mL stainless autoclave containing a certain

dx.doi.org/10.1021/cs400059n | ACS Catal. 2013, 3, 985−992

Table 1. Composition and Catalytic Performances of the As-Prepared Catalysts[a]

catalyst	χ_{Pd}[b] ($\times 10^{-3}$)	composition[c] (atom%)	R_{H^m} (mmol/h g)	time[e] (h)	yield (%)		
					EHO	EHA	EHEO
Co−B	/	$Co_{59}B_{41}$	39	5.0	86	0	14
Pd[e]	/	Pd	/	/	6	79	0
0.11 wt %-Pd/Co−B-GR	0.68	$Pd_{0.039}Co_{57.97}B_{41.99}$	78	3.0	92	0	8
0.21 wt %-Pd/Co−B-GR	1.36	$Pd_{0.078}Co_{57.90}B_{42.02}$	82	3.0	100	0	0
0.44 wt %-Pd/Co−B-GR	2.72	$Pd_{0.16}Co_{57.85}B_{41.99}$	83	3.0	100	0	0
0.22 wt %−Pd−Co−B-CR	1.35	$Pd_{0.095}Co_{74.94}B_{24.97}$	60	4.5	96	0	4
crystallized 0.21 wt %-Pd/Co−B-GR[f]	/	$Pd_{0.078}Co_{57.90}B_{42.02}$	68	4.0	66	32	2

[a]Reaction conditions: a catalyst containing 0.2 g Co, 3 mL of EHEA, 40 mL of EtOH, T = 373 K, P_{H_2} = 1.0 MPa, stirring rate = 800 rpm. [b]Nominal composition in the precursor solution, expressed in the Pd/Co molar ratio. [c]Measured by ICP analysis. [e]Reaction time needed to reach the maximum EHO yield. [e]2 mg Pd, reaction time = 4 h, 85% conversion of EHEA. [f]Obtained by treating 0.21 wt %-Pd/Co−B-GR at 673 K for 2 h in N_2.

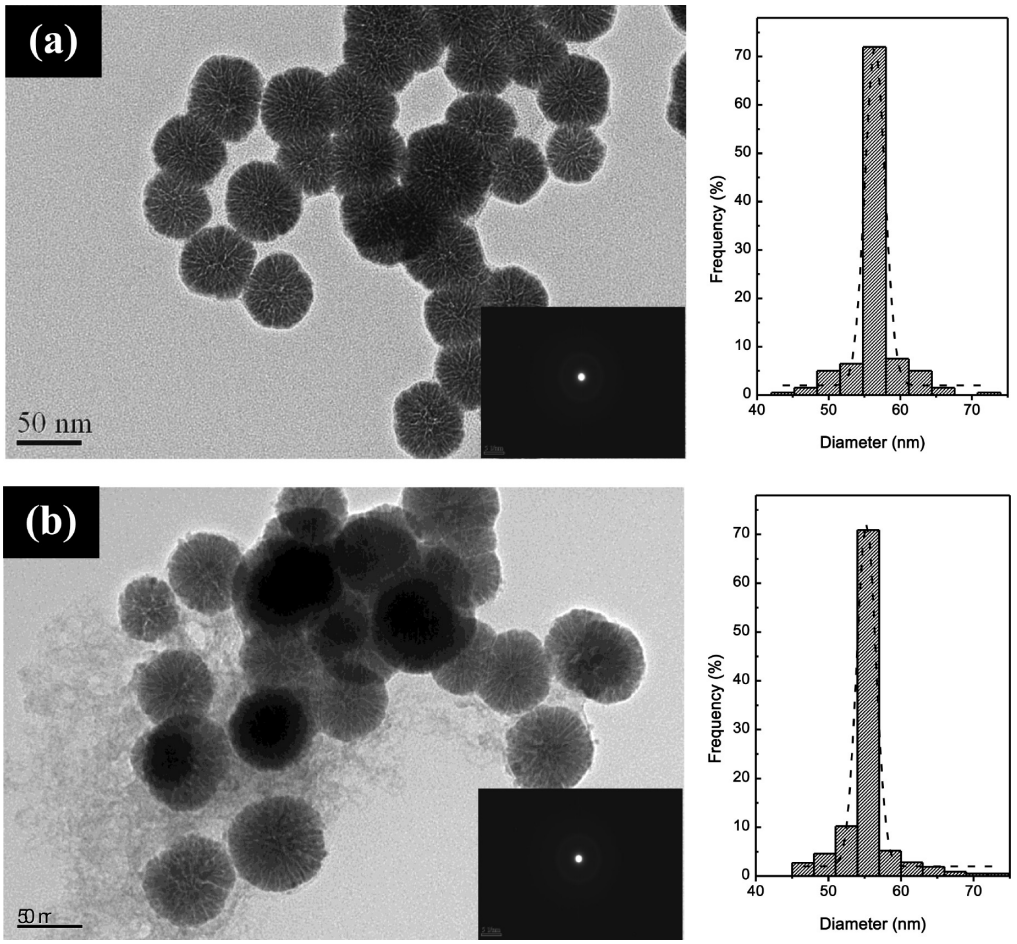

Figure 1. TEM images (*left*) and the corresponding size distribution histograms (*right*) of (a) Co−B and (b) 0.21 wt %-Pd/Co−B-GR. The insets are the SAED patterns.

amount of catalyst, 3 mL of EHEA, 40 mL of EtOH, and 1.0 MPa of H_2 at 373 K. The reaction system was stirred vigorously (800 rpm) to eliminate the diffusion effect. The reaction mixture was sampled at intervals for products analysis on gas chromatography equipped with a flame ionization detector and an EC-WAX column. All results have been reproduced and the error was limited within 5%. According to the conversion at 30 min, the specific activity (R_{H^m}/mmol h^{-1} g^{-1}) was calculated by the stoichiometric equation of chemical reaction.

RESULTS AND DISCUSSION

Structural and Electronic Characteristics. ICP analysis revealed that the bulk compositions in all the Pd/Co−B samples were very similar to those in the precursor solution (see Table 1). EDS data for 0.21 wt %-Pd/Co−B-GR confirmed the absence of Cl^-, Br^-, K^+, or Na^+ species. However, the remaining Cl^- was detected as 0.18 wt % on 0.22 wt %−Pd−Co−B-CR. These results suggest that the modified chemical reduction method and the subsequent galvanic replacement allow the removal of residual ions completely. But, the co-reduction of $CoCl_2$ and Na_2PdCl_4 with borohydride

dx.doi.org/10.1021/cs400059n | ACS Catal. 2013, 3, 985−992

causes the encapsulation of a large amount of Cl^- in the final sample due to the quick chemical reduction reaction.

The TEM image (Figure 1a) reveals that Co−B sample was present in the form of uniformly spherical nanoparticles with an average particle size around 55 nm. Crack structure with channels radiating from the center could be clearly observed from TEM image. The formation of crack channels is relative to the hydrogen released during the reduction of $[CoX_4]^{2-}$ with BH_4^-. Because of the slow reduction rate, the growth of Co−B was around the hydrogen flow and eventually evolved into nanospheres with crack channels.[18] The attached SAED image displays successive diffraction halos indicative of a typical amorphous structure.[26] The almost unchanged TEM and SAED images of 0.21 wt %-Pd/Co−B-GR (Figure 1b) show that the Pd deposition occurred with no apparent influence on the morphology, size, or amorphous structure of Co−B. It should be noted that Pd particles were invisible during a wide-scope survey of TEM observation and a typical morphology was shown in Figure 1b. The main reasons could be attributed to the low content of Pd species in the catalyst and a highly dispersed of Pd. The latter one will lead to extremely small particle sizes and poor crystalline structures, which will reduce the contrast of Pd in TEM seriously. The elemental mapping data supported our deduction as presented in Figure 2, which

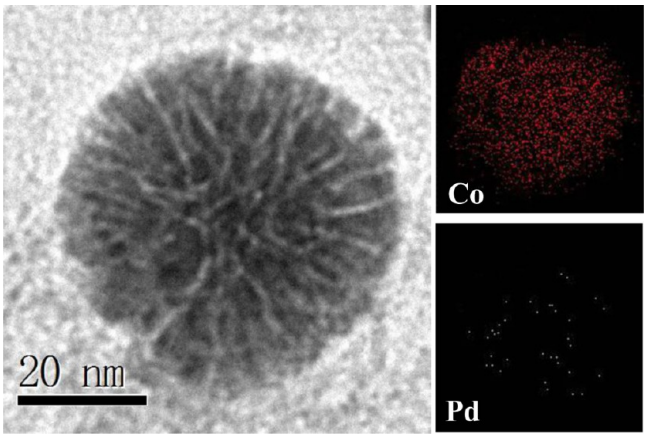

Figure 2. TEM image of a single sphere in 0.21 wt %-Pd/Co−B-GR and elemental mapping data for the sphere.

was collected from a single sphere in 0.21 wt %-Pd/Co−B-GR. The signals of Pd scattered enenly on the profile of sphere while cobalt dominated the whole area. Several HRTEM images of 0.21 wt %-Pd/Co−B-GR (Figure 3) exhibited only several Pd nanoparticles (~1.5 nm) with crystalline lattices. All the *d*-spacings were ca. 0.224 nm, which matched with {111} of Pd (fcc, PDF 88-2335) well.[27] These images provided another evidence for our deduction. These observations also clearly illustrated that the actual incorporation of Pd secondary nucleation on the surface of Co−B rather than an atomic overlayer can be achieved by GRR between Co and $[PdCl_4]^{2-}$.

The XPS spectra (Figure 4a) reveal that for all Co species in either Co−B or 0.22 wt %-Pd/Co−B−CR, the core level of Co $2p_{3/2}$ was at 778.1 eV, indicating that all Co atoms were present in metallic state.[28] However, a small amount of oxidized Co species were observed in 0.21 wt %-Pd/Co−B-GR, corresponding to the peak at 781.1 eV, possibly due to the oxidation of metallic Co by $[PdCl_4]^{2-}$. The B species in Co−B, 0.21 wt %-Pd/Co−B-GR, and 0.22 wt %−Pd−Co−B-CR were present

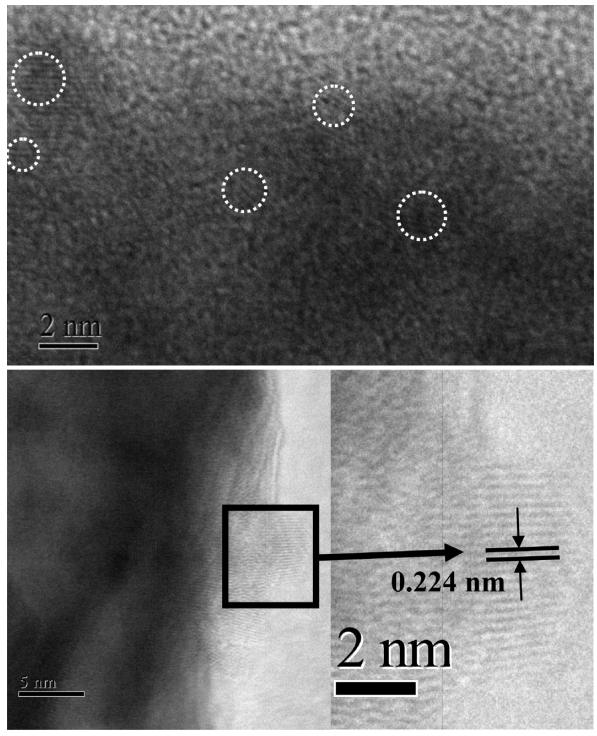

Figure 3. HRTEM image of 0.21 wt %-Pd/Co−B-GR.

in both the elemental B and the oxidized B, with B 1s BE values of around 188.1 and 191.8 eV (Figure 2b). The B 1s BE of the elemental B exceeded that of pure B (187.1 eV) by 1.1 eV,[29] further indicating that the elemental B is alloyed with the metallic Co. In alloys, partial electrons may be transferred from B to Co, as well-demonstrated previously.[18] The presence of Pd could be further confirmed by XPS analysis. Figure 4c reveal that the Pd species in both 0.21 wt %-Pd/Co−B-GR and 0.22 wt %−Pd−Co−B-CR were present in metallic state, corresponding to the BE of 335.6 and 335.1 eV in the Pd $3d_{5/2}$ core level. In comparison with the BE value of the bulk Pd (335.1 eV),[30] the BE of the Pd $3d_{5/2}$ level in 0.21 wt %-Pd/Co−B-GR shifted positively. It is well-known that the local density of states at the Fermi level decreases when the size of metal particles decreases,[31] which induce the formation of electron-deficient metallic species. Thus, the positive shift of BE in Pd $3d_{5/2}$ level is probably attributed to the effect of the reduced Pd cluster size, as demonstrated by Turner[32] and Wertheim.[33] As known, it is a very useful tool for XPS to characterize the surface electronic states, which benefits from the sensitive surface signal detection by XPS techniques. Generally speaking, up to 10 nm depth could be detected according to the Beer−Lambert Law $d = \lambda \ln(I_s/I_0)$. Taking Pd 3d and Co 2p for example, the penetration depth is about 10 nm for Pd while 5 nm for Co with Al Kα anode. Therefore, it is enough to distinguish the Pd and Co signal from noise from the XPS spectrum. According to the calculation based on XPS peak areas, the surface molar ratio of Pd to Co in 0.21 wt %-Pd/Co−B-GR was 1/15, 50 times higher than that determined by ICP (1/744, Table 1), implying that the produced metallic Pd was mainly present on the surface of Co−B. In contrast, the surface molar ratio of Pd to Co in 0.22 wt %−Pd−Co−B-CR (1/8255) was much lower than that determined by ICP (1/789, Table 1). This could be attributed to the coverage of the surface of Pd by Co−B, due to the consecutive reduction of $[PdCl_4]^{2-}$ and Co^{2+}.

dx.doi.org/10.1021/cs400059n | ACS Catal. 2013, 3, 985−992

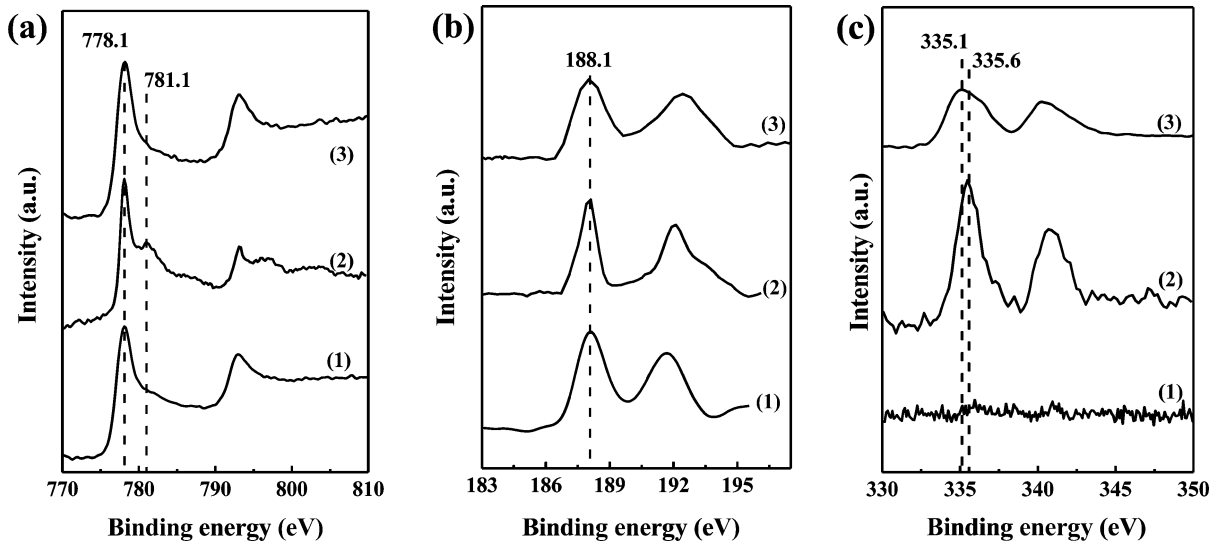

Figure 4. (a) Co 2p, (b) B 1s, and (c) Pd 3d XPS of sample surface: (1) Co−B, (2) 0.21 wt %-Pd/Co−B-GR, and (3) 0.22 wt %−Pd−Co−B-CR.

The XRD patterns presented in Figure 5 further confirmed that deposition of Pd on the surface of Co−B had no influence

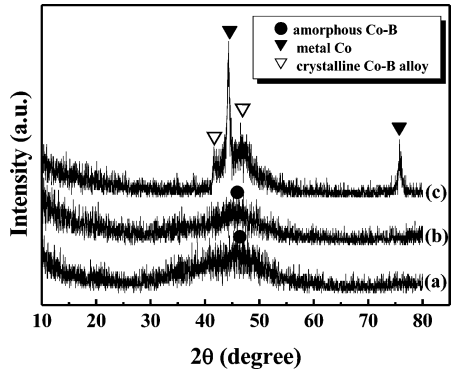

Figure 5. XRD patterns of (a) the fresh Co−B, (b) the 0.21 wt %-Pd/Co−B-GR, and (c) the 0.21 wt %-Pd/Co−B-GR sample after being treated at 673 K for 2 h in N_2 flow.

on the amorphous structure of Co−B, because only one broad peak centered at $2\theta = 44°$ was observed for both the Co−B and the as-prepared 0.21 wt %-Pd/Co−B-GR.[34] Heat treatment of the fresh 0.21 wt %-Pd/Co−B-GR sample (at 673 K in N_2 for 2 h) resulted in the appearance of several diffraction peaks corresponding to metallic Co and crystalline Co−B alloy (Figure 5c), suggesting a transformation from an amorphous structure to the crystalline structure, together with partial decomposition of Co−B amorphous alloy to metallic Co.[18] In addition, no diffraction peaks characteristic of Pd species were detected from the XRD patterns of the fresh and thermal-treated 0.21 wt %-Pd/Co−B-GR, which was most likely related to the low Pd content and the high dispersion of the Pd.

Thus, considering the results from TEM, SAED, XPS, and XRD, one can conclude that highly dispersed Pd nanoparticles on the surface of Co−B amorphous alloy can be controllably prepared by the present approach (Scheme 2).

Catalytic Performances. Figure 6 showed the changes of solution composition with reaction time during EHEA hydrogenation over Co−B, Pd, and 0.21 wt %-Pd/Co−B-GR catalysts. For Co−B amorphous alloy, except for the production of EHO, EHA and EHEO were identified as two

Scheme 2. The Formation Process of Pd/Co−B-GR

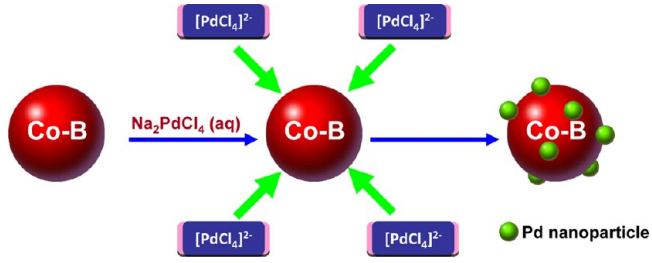

byproducts (Figure 6a). Therefore, the reaction to the saturated alcohol over Co−B can proceed through the saturated aldehyde or the unsaturated alcohol according to Scheme 1. Although EHO can be obtained with high yield (>80%) over Co−B, unsaturated alcohol (EHEO) could not be hydrogenated completely to the final product under the present conditions. This is might due to the competitive adsorption of EHO against EHEO on the catalyst surface, causing difficulty in the hydrogenation of C═C bonds at high EHO concentration. It is important to note that the main product of EHEA hydrogenation over Pd catalyst is EHA (Figure 6b). Additionally, no significant EHEO was detected throughout the hydrogenation process (Figure 6b), indicating Pd so preferred the hydrogenation of C═C bonds rather than that of C═O bonds in EHEA molecules that the present EHEA hydrogenation over Pd was a consecutive reaction. This should be attributed to the smaller *d*-bandwidth of Pd relative to Co, which weakens the four-electron repulsive interactions with the C═C bonds and thus, raising the probability of the adsorption of C═C bonds on Pd.[35] When mechanical mixtures of 0.5 mg Pd with the as-prepared Co−B was used as catalysts, the reaction profile (Figure 7a) was very similar to that for Co−B catalyst (Figure 6a), except for a slight acceleration for the hydrogenation of C═C bonds in EHEA according to the content changes of EHEA and EHA within 2 h. This further confirmed that Pd was relative inactive for the hydrogenation of C═O under the present conditions. However, incorporation of same amounts of Pd to the surface of Co−B through GRR enhanced the catalytic efficiency greatly (Table 1 and Figure 6c), apparently arising from the bi-site effect. For all of the *x* wt %-Pd/Co−B-

dx.doi.org/10.1021/cs400059n | ACS Catal. 2013, 3, 985−992

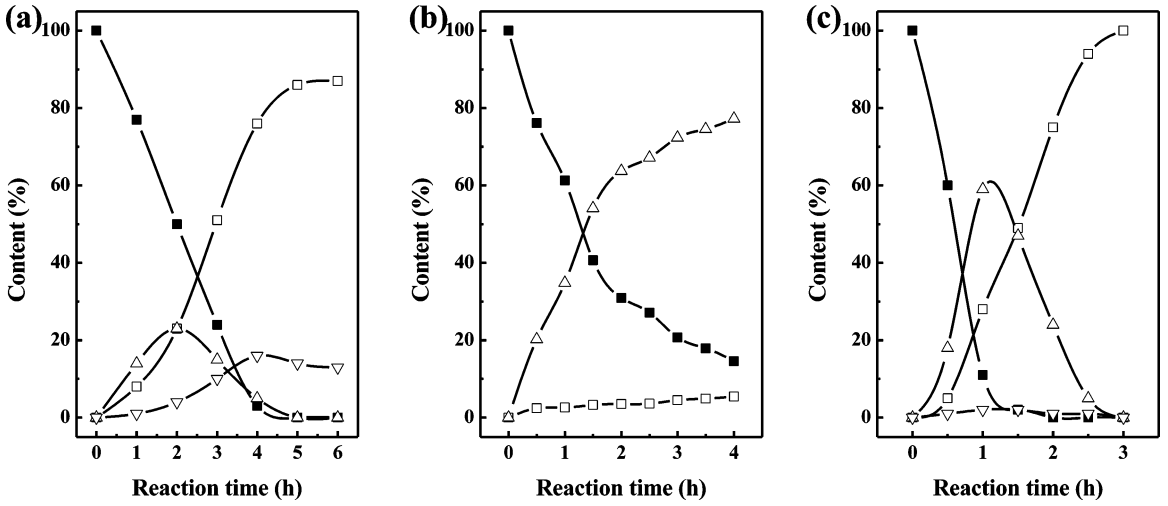

Figure 6. Reaction profiles of EHEA hydrogenation over (a) Co−B, (b) Pd, and (c) 0.21 wt %-Pd/Co−B-GR. (■) EHEA, (□) EHO, (△) EHA, and (▽) EHEO. Reaction conditions are given in Table 1.

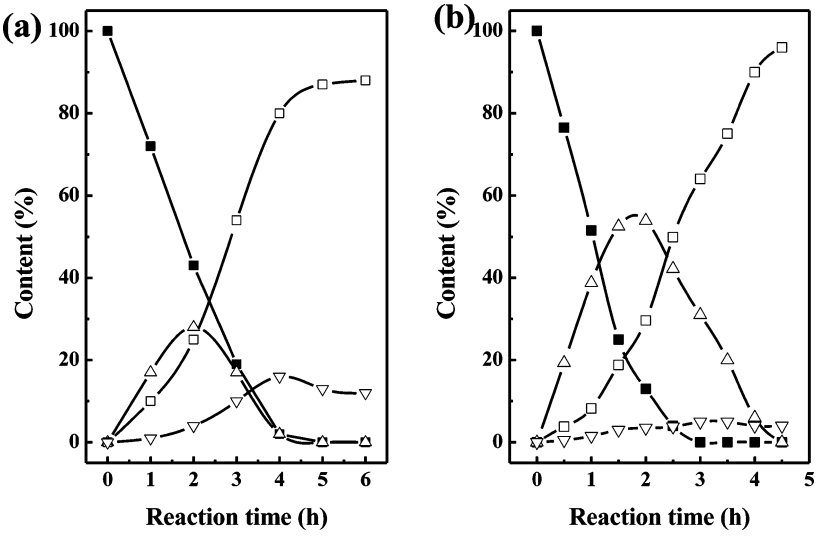

Figure 7. Reaction profiles of EHEA hydrogenation over (a) Pd (0.5 mg) + Co−B, and (b) 0.22 wt %−Pd−Co−B-CR. (■) EHEA, (□) EHO, (△) EHA, and (▽) EHEO. Reaction conditions are given in Table 1.

GR catalysts, a comparison of activity revealed that the amount of Pd had a considerable influence on the catalytic efficiency. Considering of the catalytic activity and the cost of Pd, 0.21 wt %-Pd/Co−B-GR was selected for the following studies. Abrupt decrease in activity and yield of EHO was observed for the 0.21 wt %-Pd/Co−B-GR sample treated at 673 K for 2 h in N_2 flow relative to the fresh catalyst, which was mainly due to the crystallization and decomposition of the Co−B amorphous alloy (Figure 5c).

From Figure 6c, it can be clearly seen that 0.21 wt %-Pd/Co−B-GR displayed a much different reaction pathway of EHEA hydrogenation with that over Co−B (Figure 6a). Nearly 90% of EHEA were converted within 1 h, and more than 67% of them were hydrogenated to EHA. Additionally, the content of the intermediate compound EHEO resulting from the sole hydrogenation of C═O bonds in EHEA was very low over 0.21 wt %-Pd/Co−B-GR during the whole process of the test. These observations imply that the highly dispersed Pd on the surface of Co−B is largely responsible for the hydrogenation of C═C bonds in EHEA. This should be mainly attributed to the large number of Pd active sites in 0.21 wt %-Pd/Co−B-GR due to the high exposure of Pd, which allows more hydrogen and EHEA molecules to be adsorbed. Besides, increased hydrogenation ability for C═O bonds associated with the incorporation of Pd can be found by comparing Figure 6a and Figure 6c. Figure 6a shows that 3 h was needed to hydrogenate about 20% EHA to EHO over Co−B. In contrast, 0.21 wt %-Pd/Co−B-GR could convert 60% of EHA to EHO within 2 h (Figure 6c). To rule out the influence resulted from other compounds, we tested the catalytic activity of Co−B and 0.21 wt %-Pd/Co−B-GR for the hydrogenation of EHA in a control experiment (Figure 8). Apparently, 0.21 wt %-Pd/Co−B-GR exhibits much greater activity for EHA hydrogenation than Co−B catalyst. Because Pd is relative inactive for the hydrogenation of C═O bonds under the present conditions, the catalytic activity enhancement of Co−B for the hydrogenation of C═O bonds by incorporation of Pd indicated that there is a synergetic effect between Pd and Co, which can be demonstrated by H_2-TPD results. Figure 9 shows the H_2-TPD curves of Pd, Co−B and 0.21 wt %-Pd/Co−B-GR catalysts. In the trace of Pd catalyst (Figure 9a), only one desorption peak at low temperature (353 K) was observed, which can be ascribed

dx.doi.org/10.1021/cs400059n | ACS Catal. 2013, 3, 985−992

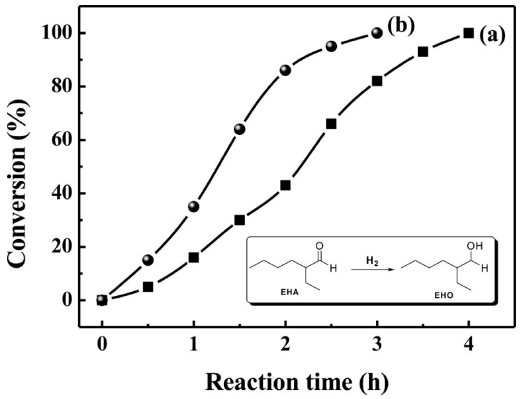

Figure 8. Time−conversion curves of EHA hydrogenation to EHO over (a) Co−B and (b) 0.21 wt %-Pd/Co−B-GR. Reaction conditions: a catalyst containing 0.2 g of Co, 3 mL of EHA, 40 mL of EtOH, T = 373 K, P_{H_2} = 1.0 MPa, stirring rate = 800 rpm.

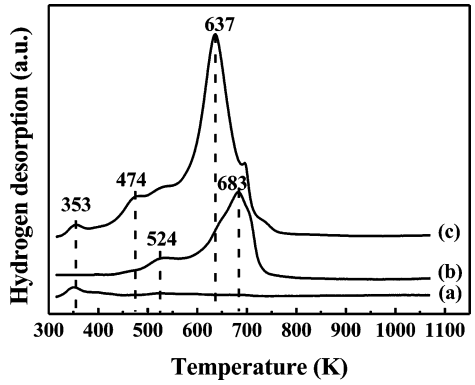

Figure 9. H_2-TPD profiles of catalysts: (a) Pd, (b) Co−B, and (c) 0.21 wt %-Pd/Co−B-GR. The signals of (b) and (c) are normalized based on unit mass Co.

to the hydrogen species from the surface of metallic Pd.[36] For Co−B catalyst (Figure 9b), the H_2-TPD profile reveals a principal desorption peak located at 683 and a small peak at 524 K, suggesting that Co−B contained uniform Co active sites. Besides the above-mentioned three desorption peaks, two obvious peaks at 474 and 637 K appeared in 0.21 wt %-Pd/Co−B-GR (Figure 9c). More interestingly, the great amount of hydrogen desorbed at 637 K resulted in nonstoichiometric H/M ratio. The hydrogen species desorbed at these additional temperatures could be due to the spillover hydrogen. That is, the active hydrogen formed on the surface of Pd would spillover to and store on the surface of Co.[37] Xia et al.[38] studied Pd−Cu and Wu et al.[25] studied Pd−Ni, and came to similar conclusions, i.e., that hydrogen was adsorbing on Pd and spilling over onto Cu or Ni. In terms of heterogeneous catalysis, spillover is a well-documented phenomenon,[37] which can enhance H_2 activation ability and thus improve the hydrogenation activity. Our H_2-TPD experiments confirmed that the dispersion of Pd on the surface of Co−B could provide a much-higher concentration of active hydrogen via hydrogen spillover from Pd to Co, which gives rise to the fast hydrogenation of C═O. Despite similar Pd content, 0.21 wt %-Pd/Co−B-GR was distinctly superior to the reference 0.22 wt %−Pd−Co−B-CR, since complete conversion of EHEA to EHO can be achieved within 3 h over the former (Figure 6c) while 4.5 h was needed to convert EHEA to EHO with 96% yield over the latter (Figure 7b). The superior catalytic properties of 0.21 wt %-Pd/Co−B-GR should be mainly attributed to their larger number of exposed Pd relative to that in 0.22 wt %−Pd−Co−B-CR, as demonstrated by the aforementioned XPS analysis, which would allow more favorable hydrogenation of C═C bonds by metallic Pd.

We compared the catalytic efficiencies of 0.21 wt %-Pd/Co−B-GR with the classical systems generally used in industry, including Cu/Zn/Al, Cu−Cr and Cu−Ni. As shown in Figure 10, the as-prepared 0.21 wt %-Pd/Co−B-GR exhibited much

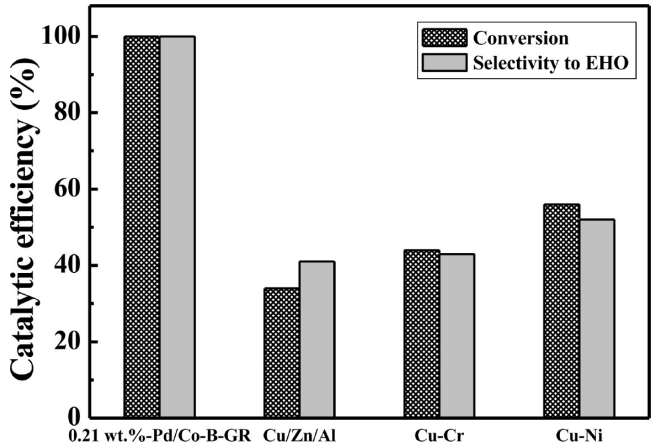

Figure 10. EHEA conversion and selectivity to EHO obtained on 0.21 wt %-Pd/Co−B-GR, Cu/Zn/Al, Cu−Cr and Cu−Ni during EHEA hydrogenation. Reaction conditions: a catalyst containing 0.2 g of Co or Cu, 3 mL of EHEA, 40 mL of EtOH, T = 373 K, P_{H_2} = 1.0 MPa, stirring rate = 800 rpm, t = 3 h.

greater EHO yield compared with the Cu-based catalysts. The superior catalytic properties of the as-prepared catalyst can be attributed to the bi-site effect of Pd/Co−B in which both metals play specific role with respect to the reactants.

The recycling test (Figure 11) shows that 0.21 wt %-Pd/Co−B-GR catalyst can be use repetitively 5 times with a slight loss of activity (10%). ICP analysis reveals that no leaching of Pd or Co species could be detected in the reaction mixtures during repetitive runs, implying that this catalyst was stable against the chelating effect of the reactant and product. Meanwhile, no significant agglomeration of Pd nanoparticles could be observed

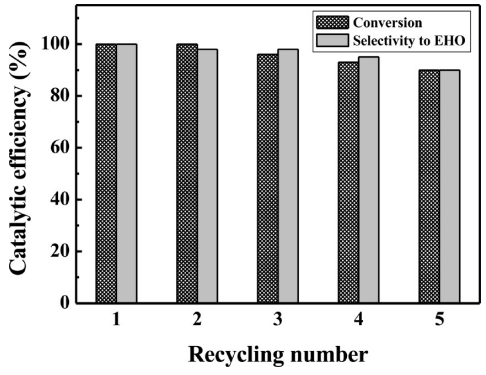

Figure 11. Recycling test of 0.21 wt %-Pd/Co−B-GR catalyst for EHEA hydrogenation. Reaction conditions: a catalyst containing 0.2 g of Co, 3 mL of EHEA, 40 mL of EtOH, T = 373 K, P_{H_2} = 1.0 MPa, stirring rate = 800 rpm, t = 3 h.

dx.doi.org/10.1021/cs400059n | ACS Catal. 2013, 3, 985−992

over the reused catalyst after 5 consecutive runs (Figure 12a). At the end of the fifth cycle, the weight decrease of catalyst was

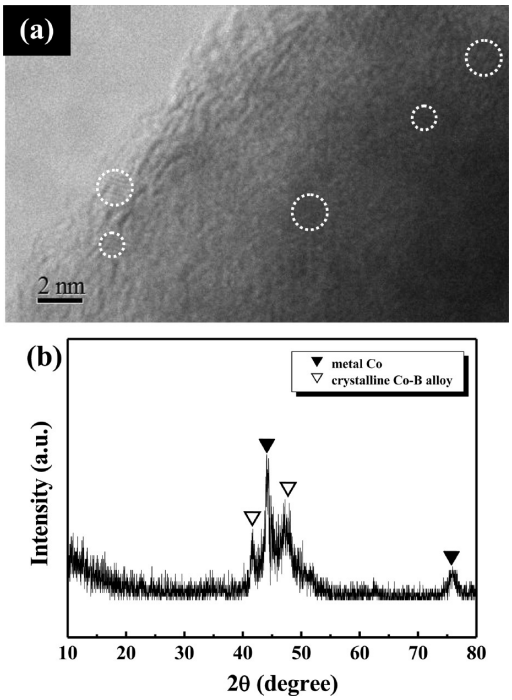

Figure 12. (a) HRTEM image and (b) XRD pattern of 0.21 wt %Pd/Co−B-GR after five consecutive runs for EHEA hydrogenation. The reaction conditions are listed in Figure 10.

4.5% while no significant change in the composition of catalyst was determined by ICP analysis, suggesting that the loss of catalyst during the washing procedure is one factor responsible for the decrease of the EHEA hydrogenation during the recycling test. Additionally, partial crystallization occurred for the spent 0.21 wt %-Pd/Co−B-GR catalyst (Figure 12b), which was also responsible for its deactivation.

CONCLUSIONS

In summary, highly dispersed Pd on the surface of Co−B amorphous alloy could be achieved through a two-step approach by using galvanic replacement reaction. During the liquid-phase hydrogenation of 2-ethyl-2-hexenaldehyde to 2-ethyl-1-hexanol, such novel Pd/Co−B catalysts delivered excellent activity than that associated with the reference monometallic catalysts, due to the significant bi-site effect. Our findings demonstrate the advantages of the present method, making it possible to prepare other efficient bimetallic catalysts and giving new levels of control over the structures and catalytic properties.

AUTHOR INFORMATION

Corresponding Author

*Tel: +86-21-64322272. Fax: +86-21-64322272. E-mail: lihui@shnu.edu.cn.

Notes

The authors declare no competing financial interest.

ACKNOWLEDGMENTS

This work is supported by the National Natural Science Foundation of China (21273149, 20703011), the Program for New Century Excellent Talents in University (NCET-11-1052), and the Shanghai Science & Technology and Education Committee (11JC1408900, 12490502800, 10SG41, 12YZ084).

REFERENCES

(1) Kirshenbaum, I.; Inchalik, E. J. In *Kirk-Othmer Encyclopedia of Chemical Technology*; 3rd ed.; Grayson, M., Eckroth, D., Eds.; John Wiley & Sons: New York, 1981; Vol. *16*, pp 637−653.
(2) Novak, L.; Nebesh, E. *Ind. Eng. Chem. Res.* **1991**, *30*, 2514.
(3) Reich, M.; Schneider, K. US 3491159 1970.
(4) Schröder, U.; Andersson, B. *J. Catal.* **1991**, *132*, 402.
(5) Wiedemann, K.; Broich, F. DE 931827 1955.
(6) Pickup, K. G. GB 19600625 1962.
(7) Cooper, L. E. FR 1349816 1964.
(8) Klement, K.; Willens, R. H.; Duwez, P. *Nature* **1960**, *187*, 869.
(9) Van Wonterghem, J.; Mørup, S.; Koch, C. J. W.; Charles, S. W.; Well, S. *Nature* **1986**, *322*, 622.
(10) Molnar, A.; Smith, G. V.; Bartok, M. *Adv. Catal.* **1989**, *36*, 329.
(11) Chen, Y. *Catal. Today* **1998**, *44*, 3.
(12) Deng, J. F.; Li, H. X.; Wang, W. J. *Catal. Today* **1999**, *51*, 113.
(13) Pei, Y.; Zhou, G. B.; Luan, N.; Zong, B. N.; Qiao, M. H.; Tao, F. *Chem. Soc. Rev.* **2012**, *41*, 8140.
(14) Li, H. X.; Li, H.; Zhang, J.; Dai, W. L.; Qiao, M. H. *J. Catal.* **2007**, *246*, 301.
(15) Li, H.; Yang, H. X.; Li, H. X. *J. Catal.* **2007**, *251*, 233.
(16) Li, H.; Liu, J.; Xie, S. H.; Qiao, M. H.; Dai, W. L.; Li, H. X. *J. Catal.* **2008**, *259*, 104.
(17) Li, H.; Liu, J.; Yang, H. X.; Li, H. X. *J. Mater. Res.* **2009**, *24*, 3300.
(18) Zhu, Z. H.; Ma, J. Q.; Xu, L.; Xu, L.; Li, H. X. *ACS Catal.* **2012**, *2*, 2119.
(19) Freifelder, M. In *Practical Catalytic Hydrogenation: Techniques and Applications*; Wiley-Interscience: New York, 1971; pp 127−449.
(20) Wang, D. S.; Li, Y. D. *Adv. Mater.* **2011**, *23*, 1044.
(21) Son, S. U.; Jang, Y.; Park, J.; Na, H. B.; Park, H. M. *J. Am. Chem. Soc.* **2001**, *126*, 5026.
(22) Li, H.; Zhu, Z. H; Liu, J.; Xie, S. H.; Li, H. X. *J. Mater. Chem.* **2010**, *20*, 4366.
(23) Lu, X.; Chen, J.; Skrabalak, S. E.; Xia, Y. *Proc. Inst. Mech. Eng., Part N* **2007**, *221*, 1.
(24) Wang, S.; Lin, W.; Zhu, Y.; Xie, Y.; McCormick, J. R.; Huang, W.; Chen, J. G. *Catal. Lett.* **2007**, *114*, 169.
(25) Wu, Z.; Zhang, M.; Zhao, Z.; Li, W.; Tao, K. *J. Catal.* **2008**, *256*, 323.
(26) Martens, K. S.; Parton, J. A.; Vercruysse, R.; Jacobs, K.; Maier, P. A. *Catal. Lett.* **1996**, *38*, 209.
(27) Mazumder, V.; Sun, S. *J. Am. Chem. Soc.* **2009**, *131*, 4588.
(28) Mclntyre, N. S.; Cook, M. G. *Anal. Chem.* **1975**, *47*, 2208.
(29) Li, H.; Li, H. X.; Dai, W. L.; Wang, W. J.; Fang, Z. G.; Deng, J. F. *Appl. Surf. Sci.* **1999**, *152*, 25.
(30) Weightman, P.; Andrews, P. T. *J. Phys. C: Solid State Phys.* **1980**, *13*, L815.
(31) Gordon, B.; Cyrot-Lackmann, F.; Desjonquières, M. C. *Surf. Sci.* **1977**, *68*, 359.
(32) Turner, M.; Golovko, V. B.; Vaughan, O. P. H.; Abdulkin, P.; Berenguer-Murcia, A.; Tikhov, M. S.; Johnson, B. F. G.; Lambert, R. M. *Nature* **2008**, *454*, 981.
(33) Wertheim, G. K.; DiCenzo, S. B. *Phys. Rev. B* **1988**, *37*, 844.
(34) Yokoyama, A.; Komiyama, H.; Inoue, H.; Masumoto, T.; Kimura, H. M. *J. Catal.* **1981**, *68*, 355.
(35) Delbecq, F.; Sautet, P. *J. Catal.* **1995**, *152*, 217.
(36) Ilinich, O. M.; Gribov, E. N.; Simonov, P. A. *Catal. Today* **2003**, *82*, 49.
(37) Conner, W. C.; Falconer, J. L. *Chem. Rev.* **1995**, *95*, 759.
(38) Xia, S.; Yuan, Z.; Wang, L.; Chen, P.; Hou, Z. *Appl. Catal., A* **2011**, *403*, 173.